Journal of the Energy Institute 123 (2025) 102314

Contents lists available at ScienceDirect

Journal of the Energy Institute

journal homepage: www.elsevier.com/locate/joei

Numerical investigation on the combustion characteristics of premixed NH_3-air flames using gliding arc plasma

Ziyu Wang, B. Aravind *, Syed Mashruk, Agustin Valera-Medina

College of Physical Sciences and Engineering, Cardiff University, Wales, CF24 3AA, UK

ARTICLE INFO

Handling Editor: Dr. Paul Williams

Keywords:
Ammonia
Non-equilibrium plasma
Carbon-free combustion
Numerical model
Emission

ABSTRACT

In this study, a numerical model is developed to predict the combustion characteristics of gliding arc plasma (GAP) assisted ammonia (NH_3)-air mixture, integrating ZDPlasKin and Chemkin. To the best of the authors' knowledge, this is the first validated model capable of accurately predicting NO emissions from GAP-assisted NH_3-air combustion. Initially, three well-known plasma mechanisms are evaluated against non-reacting GAP experiments to assess their effectiveness in modelling NH_3-air plasma chemistry. The most accurate mechanism is then coupled with an optimized combustion mechanism to improve NO prediction accuracy. The results indicate that NH_2 radical formation is enhanced by approximately 7 % at a reduced electric field of 30 Td, playing a crucial role in NO reduction. Additionally, NH_2 is primarily generated through two key reactions: $O(^1D) + NH_3 \rightarrow OH + NH_2$ and $N_2(A) + NH_3 \rightarrow NH_2 + N_2 + H$, occurring before combustion. Furthermore, increasing plasma power significantly accelerates NO consumption by promoting the formation of excited NH_3 states ($NH_3(e_1)$, $NH_3(e_2)$), which enhance NH_2 and NH radical production. Sensitivity analysis reveals that NH_2 exhibits a 52.1 % sensitivity to the reaction $N(^2D) + NH_3 \rightarrow NH_2 + H + N_2$ at 90 Td, highlighting its dominant role in NO reduction.

1. Introduction

Ammonia (NH_3) is gaining significant attention as a promising green fuel due to its carbon-free combustion, high energy density comparable to fossil fuels (22.5 MJ/kg) [1], and cost-effective storage, positioning it as a viable solution to the current energy crisis [2]. Despite these advantages, NH_3 has high NO_x emissions due to its inherently low flame temperature, low laminar combustion rate, and low flammability [3]. To circumvent these issues, co firing of NH_3 with highly reactive fuels [4], such as methane [5] and hydrogen [6], staged combustion [7], humidification [8], plasma assisted combustion [9] etc. are commonly adopted techniques.

Among these techniques, plasma assisted combustion [10], is relatively new strategy and, with great potential to enhance the flame stability and other combustion characteristics [9,11]. Although its impact on NH_3 combustion is comparatively less explored, recent studies [12–14] have shown that plasma can significantly address the drawbacks of NH_3 as a future fuel [15]. However, plasma assisted combustion of NH_3 does not alter the primary NO generation pathway, where HNO is involved in 70 % of the reaction [16]. This suggests that a careful analysis of the reaction pathways involved in plasma-assisted combustion of NH_3 is essential to understand NO_x consumption through the production of NH radicals [17]. The dielectric barrier discharge (DBD) assisted NH_3 combustion on the premixed NH_3-H_2-air, revealed that NO_x emissions increases with the plasma in laminar/turbulent flames [18]. While Ju et al. [14] found that NO has been reduced significantly using gliding arc plasmas (GAP), by promoting the NO consumption reactions.

In plasma assisted combustion modelling, many researchers have made a considerable contribution in DBD and nanosecond repetitively pulsed discharges (NRP) [16–22]. Faingold et al. [19] conducted a detailed parametric studies on the effect of pulse repetition frequency, number of pluses of NRP on the ignition delay time (IDT) characteristics of NH_3-O_2-He mixtures. Shahsavari et al. [20] investigated the impact of NRP on flame characteristics. They found that the pulse energy density increasing in the range of 0–20 mJ/cm^3, at a given reduced electric field, decreases the IDT. In 2019, Mao et al. proposed a numerical model to predict the Ignition enhancement of CH_4-O_2-He mixtures under NRP and DC discharges [21]. Recently, Zhong et al. developed a robust kinetic model for plasma combustion of NH_3-O_2-N_2 that are validated with the experiments [22]. The same plasma mechanism was used by Mao et al.

* Corresponding author.
E-mail address: balakrishnana4@cardiff.ac.uk (B. Aravind).

https://doi.org/10.1016/j.joei.2025.102314
Received 6 July 2025; Received in revised form 16 September 2025; Accepted 29 September 2025
Available online 30 September 2025
1743-9671/© 2025 The Authors. Published by Elsevier Ltd on behalf of The Energy Institute. This is an open access article under the CC BY license (http://creativecommons.org/licenses/by/4.0/).

[23] for DBD-promoted ignition delay of NH_3-air and in the analysis of NO formation mechanisms. The IDT and NOx emission mechanisms of NH_3-air by NRP were similarly investigated by Taneja et al. [24]. Shahsavari et al. [25] constructed a specific mechanism for the action of NRP and hydrogen on the combustion of ammonia, verifying the change in temperature under specific conditions.

Although numerous experimental and numerical studies [19,20,22–27] have investigated NRP and DBD for NH_3 ignition and NO formation, research on GAP for ammonia combustion has largely remained experimental [12,14,18,28]. Nevertheless, Compared with DBD and NRP, the rotating gliding arc plasma provides broad volumetric coverage and can be directly incorporated into the combustion zone, making it highly promising for enhancing combustion. Meanwhile, GAP also features a combination of high energy density and thermal effects, enabling continuous and stable discharge that effectively promotes chemical reactions in combustion. Recent studies have shown that GAP plasma combustion significantly reduces NO_x emissions, drawing increasing attention from the research community [14,28,29]. However, the underlying mechanisms of NO reduction in GAP remain unclear, and existing experimental results lack comprehensive interpretation and analysis.

In this work, for the first time, numerical model is developed to study the GAP-assisted combustion characteristics of NH_3-air mixture. Initially, different plasma mechanisms are compared, the most suitable one for GAP is selected based on experimental validation. This is followed by the development of a combustion mechanism integrated with the plasma mechanism. Finally, the mechanism behind the NO emission reduction under the influence of GAP is analysed in detail.

2. Numerical methods and model validation

In order to validate the numerical method, GAP experiments are conducted to comprehend the effect of GAP on the NH_3 conversion rate for non-reacting cases. The details of the experiment setup are shown in the Supplementary Material Fig. S1. Different ratios of NH_3-air are injected from the tube, and the gas mixture is ionized by an arc formed by the high-voltage electrode. The "fresh gas" is taken above the electrode and the volume fraction of NH_3 is measured using Agilent 990 microGC. The chemiluminescence spectrum of the discharge at the burner's exit and 10 cm from its central axis was recorded using a flexible AvaSpec-ULS spectrometer, where the stray light (0.19–1.0 %) represented the main source of error. This method for determining electron temperature based on the H-α/H-β spectral line intensity ratio has relative errors of only ±0.017 % [30]. Therefore, the potential overall uncertainty is estimated to below 1.017 %. The typical temporal evolution of the voltage and current waveform of GAP in the present study is shown in the Supplementary Material Fig. S2. As evident from Fig. S2 that voltage shows a periodic jagged shape, and current spikes are observed at each breakdown at the smallest gap. This breakdown type GAP is observed for many plasma assisted combustion studies [28]. In GAP, both spark-type discharge and glow-type discharge are observed [12], In the present study, current reaches above 1 A and below 0.5 A are termed as spark and glow discharges.

2.1. Numerical method

This study adopts a numerical methodology similar to that proposed by Crispim et al. for modelling the GAP [31]. The simulation is divided into two domains, as shown in Fig. 1. The first domain, 0–t_1, represents the discharge length or residence time. During this period, the arc initiates at the minimum gap, peaks in current, propagates helically, elongates, and eventually breaks as the current drops to zero. The minimum clearance between the conical electrode and the tube wall is 2.5 mm, with a charging length of 14 mm from this location to the apex. This discharge time is calculated from the voltage-current curve. The second domain, t_1–t_2, is termed as the afterglow discharge. The

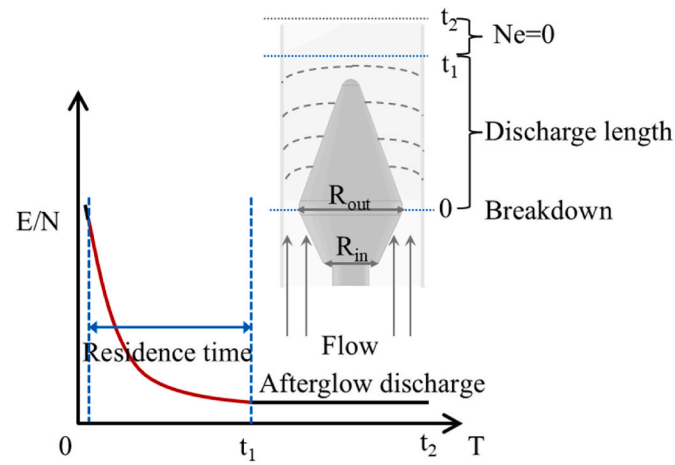

Fig. 1. Theory of gliding arc plasma.

discharge power is maintaining between 130 and 150 W, and the frequency of plasma is 11 kHz. The discharge time is between 4 and 7 ms, depends on the gas flow rate. The plasma chemistry in the afterglow region is significantly different from that of the plasma glow [23]. However, the afterglow retains most of the plasma properties.

To simplify the calculations, the reduced electric field and electron density are estimated as period averages using the voltage-current characteristic curves. This study was carried out using a dual-swirl plasma-assisted burner at CEAT, Cardiff University. Further details of this burner are available in Wang et al. [29] and Aravind et al. [32]. In the ionization region, the initial gas mixture consists of $NH_3/N_2/O_2$. The electron density is calculated using Eq. (1) [33]:

$$Ne = J_{av}/e\mu_e E \tag{1}$$

In Eq. (1), Ne is the current density, J_{av} is the ratio of current to cross-sectional area, A/cm^2. The electron mobility (μ_e) is calculated from BOLSIG+, derived from collision interface data with initial E/N intensity, divided by initial gas density, cm^2/Vs. E is electric field, V/cm.

In this study, the current curve provides the data between 0.1 and 0.11 A, the average electron conduction current density was calculated to 1–1.16 A/m^{-2}, the electric field (E) within the discharge region measured 2.1 kV/cm, the electron mobility (μe) is calculated at 500 cm^2/V. The electron density averaged across the conical electrode was estimated to be 5.7×10^{12} - 6.4×10^{12} cm^{-3}.

The E/N is determined from the experimental voltage, electrode gap length and gas density [28]. The initial gas density is estimated by initial pressure and temperature, 2.4×10^{19} cm^{-3}. The voltage is estimated at 1.8–4.5 kV. In this study, the E/N is 30–90 Td. This range of reduced electric field strength is similar to that reported by Dong et al. [34].

The initial electron temperatures were preliminary determined based on spectral measurements. Spectral measurements at different mixture ratios are shown in Fig. 2. The electron temperature of the plasma is estimated using Eq. (2) based on the spectral characteristics observed in experiments [30]. The electron temperature is used as an initial parameter in order to assume Maxwellian energy distribution for electrons; the value of reduced field is calculated in this case to satisfy electron energy balance. This estimation can enhance the numerical method for different NH_3-air ratios.

$$In\ (I_{32}/I_{42}) = In\ (\upsilon_{32}/\upsilon_{42}) + 1.08 + h(\upsilon_{42}-\upsilon_{32})/\ (kT_e) \tag{2}$$

Where T_e is the electron temperature in Kelvin. I_{32} and I_{42} are the intensity of H-α(486.1 nm), H-β(656.3 nm). υ_{32} and υ_{42} are frequencies of radiation initiated in nm. h is the Planck constant in J·s. k is Boltzmann constant, J/K. The system is assumed to be in local thermal equilibrium when the electron temperature of the plasma ranges between 4000 and 64,000 K. The electron temperature is used as an initial parameter in

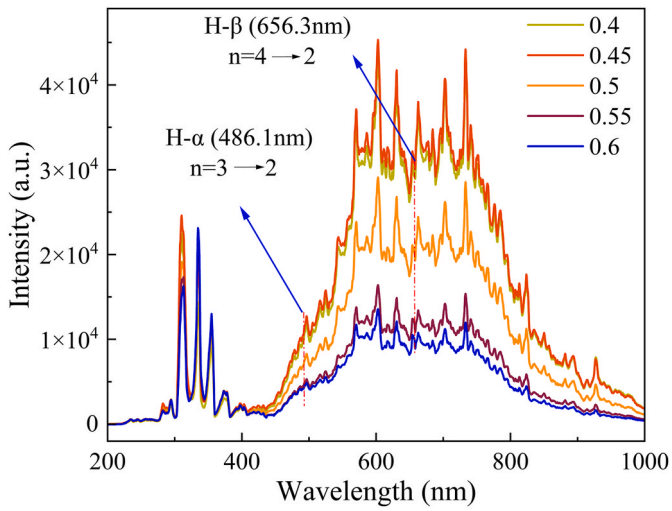

Fig. 2. Spectra of plasma at different NH_3 ratios.

order to assume Maxwellian energy distribution for electrons; the value of reduced field is calculated in this case to satisfy electron energy balance.

As a transient property, the mixture density (ρ_{mix}) dynamically adjusts to real-time composition variations, computed through the component-based formulation in Eq. (3).

$$\rho_{mix} = \frac{1}{N_A}\sum_i M_i \cdot n_i \tag{3}$$

Where i represents different species, [NH_3, N_2, O_2 …]. M_i denotes the molar mass of species i. The number density of each component is represented by n_i. N_A is Avogadro's constant, 6.022×10^{23} mol^{-1}.

The GAP reactor exhibits substantially higher gas temperatures, observed by Dong et al. [34]. Compared to conventional DBD reactors, representing a fundamental operational difference between these plasma systems. Consequently, the GAP generated thermal effects on gas mixtures should be explicitly considered in the analysis. When it taken into account, the gas temperature (T_{gas}) can be determined through the heat transfer equation (4) under the physical condition of adiabatic equidistant approximation [35].

$$\frac{N_{gas}}{\gamma - 1}\frac{dT_{gas}}{dt} = \sum_{i=1}^{i_{max}} \pm \delta\varepsilon_i \cdot R_i + P_{elast} \cdot [N_e] + P_{ex} \tag{4}$$

$$\lambda_{mix} = \frac{1}{\rho_{mix}}\sum_i (\lambda_i \cdot C_i) \tag{5}$$

$$c_{p,mix} = \sum_i N_i \cdot \frac{\gamma_i}{\gamma_i - 1} \tag{6}$$

$$P_{ex} = \frac{N_u \cdot \lambda \cdot (T_{gas} - T_{wall})}{R_{out}^{\ 2}} \tag{7}$$

$\sum_{i=1}^{i_{max}} \pm\delta\varepsilon_i \cdot R_i$ represents the heat of chemical reactions; P_{elast} corresponds to Joule heating induced by electron current, associated with elastic electron-neutral collisions (this term is computed using the BOLSIG + solver. P_{ex} is a user-defined heat source that can be arbitrarily specified in equation (7). The symbol λ is used for the gas-phase thermal conductivity. c_p denotes the specific heat capacity at constant pressure. N_i and γ_i are the density and specific heat ratio of component i, respectively. C_i represents the concentration of the i-th gas species (where i is defined consistent with Equation (3)). The Nusselt number is fixed at $Nu = 8$ for this analysis. The effective thermal conductivity (λ) of the gas mixture is calculated as a weighted average of the constituent species (NH_3, O_2, and N_2 …) based on their respective concentrations. The reactor wall temperature (T_{wall}) is held constant at the initial reaction temperature throughout the simulation. The system geometry is characterized by reactor radius R_{out}.

2.2. Model validation

The method of coupling ZDPlasKin [35] with Chemkin [36] has been generally validated by numerous studies, demonstrating its effectiveness in accurately simulating plasma-assisted combustion processes, including the evolution of chemical species and changes in gas temperature [22].

The plasma mechanisms of NH_3-air mixtures under plasma conditions have also been the subject of several studies [23–25]. Taneja et al. [24] assembled a reaction mechanism comprising 53 species and 383 reactions for NRP. Shahsavari et al. [25] assembled a plasma reaction mechanism comprising 61 species and 790 reactions. A plasma kinetic mechanism was constructed by integrating the NH_3-O_2-He reaction mechanism proposed by Faingold et al. [19]. Mao et al. [23] provided a plasma mechanism which includes 77 species and 894 reactions. A plasma mechanism involving NH_3-O_2-N_2 was utilized in DBD.

Although several mechanisms have been developed for NRP [24,25], no mechanism is currently available for GAP-assisted combustion of NH_3. As an initial step toward identifying the most suitable mechanism for GAP, the performance of models proposed by Mao et al. [23], Taneja et al. [24], and Shahsavari et al. [25]is compared with the present experimental results on GAP-assisted NH_3 conversion in non-reacting cases. The NH_3 conversion rate was calculated from the initial NH_3 volume fraction and the sampled ammonia volume fraction [37].

It is evident from Fig. 3 that mechanism proposed by Mao et al. [23] demonstrates good agreement with the present experiments and is therefore selected for the subsequent simulations. Following the selection of a suitable mechanism for GAP, the plasma mechanism of Mao et al. [23] is combined then with the NH_3 combustion mechanism proposed by Alnasif et al. [38,39].

During the coupling process, Alnasif's mechanism serves as the host, while Mao et al.'s mechanism functions as the donor. All plasma-related reactions from Mao's mechanism are integrated into Alnasif's mechanism, with overlapping reactions and species carefully removed. The equivalence ratio is defined as follows:

$$\Phi = \frac{(F/O)_{real}}{(F/O)_{stoichiometric}} \tag{8}$$

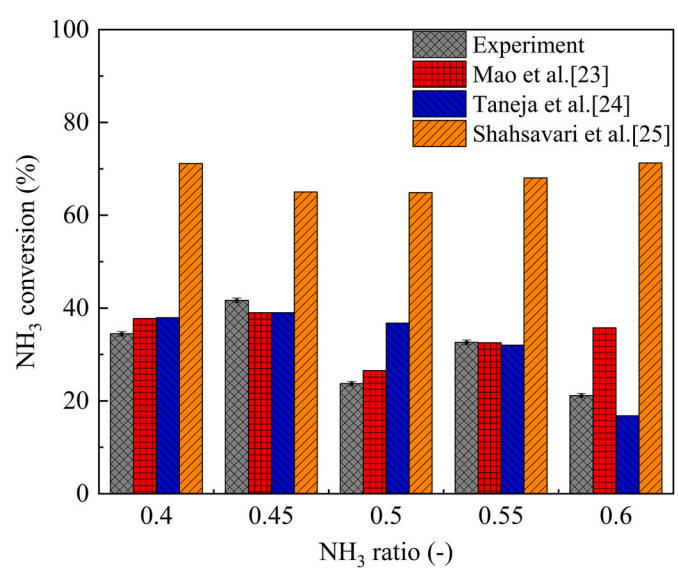

Fig. 3. Validation of NH_3 plasma mechanism suitable for GAP.

Here, $(F/O)_{real}$ is the actual molar of fuel to oxidizer, $(F/O)_{stoichiometric}$ is the molar of fuel to oxidizer under stoichiometric conditions

Then is the performance of the coupled mechanism on NO_x prediction is compared with the various GAP assisted NH_3 combustion experimental results of Ju et al. [14] and Tang et al. [28], as shown in Fig. 4. Notably, the experimental data are all based on NO_x studies of premixed NH_3–air flames in a plasma-assisted swirl burner. For plasma-assisted ammonia/air flames, the NO peak appears around $\phi = 0.8$ and gradually decreases as the equivalence ratio increases. Under fuel-rich conditions, the obtained NO is approximately zero. The numerical simulation results correspond well with this trend. Experimental results are well captured by the Mao–Alnasif mechanism. The deviation of the mechanism from the experiment is less than 5 % When ϕ is 0.7–0.82 and 0.95–1.0.

3. Result and discussion

3.1. Effect of GAP on density of main species

This section discusses the variation in gas density and temperature of the main components of premixed NH_3-air gas under GAP at E/N = 30 Td. This E/N value is selected for analysis as it falls within the estimated range for the GAP experiments.

The transformation of gas species during the gliding arc plasma actuation can be divided into two distinct phases as shown in Fig. 5(a) and (b). The first phase involves gas ionization during the discharge phase which is up to 6.25 ms, where a high electron density facilitates collisions between high-energy electrons and gas molecules. These interactions transfer energy to the gas molecules, exciting them from their ground or low-excited states to vibrationally excited states [37]. This responds to the fact that the densities of NH_3, nitrogen (N_2), and oxygen (O_2) all decrease significantly during the residence time in Fig. 1. As shown in Fig. 5 (a), after plasma ionization, the final gas density of N_2 and O_2 decreased by 26 % and 44 % respectively. The final observed change in density is 26 % for N_2 and 44 % for O_2. Furthermore, oxygen atoms present the highest percentage of H, N and O. It is presumed that this is since oxygen has a lower ionization (12.07 eV) and dissociation energy (5.12 eV) and is more easily ionized and dissociated [40]. Oxygen atoms, being chemically active, can be generated via various reaction pathways. During the discharge phase, the arc raises the gas temperature, which is further governed by the specific heat, leading to a gradual temperature increase, as shown in Fig. 5 (a). It is also observed that after the current disappears, the temperature decreases before eventually rising by approximately 100 K. Some intermediate components are generated during the plasma process as shown in Fig. 5 (b). The final gas composition of NH_2 and OH has increased by 6.75 % and 4.74 %, respectively.

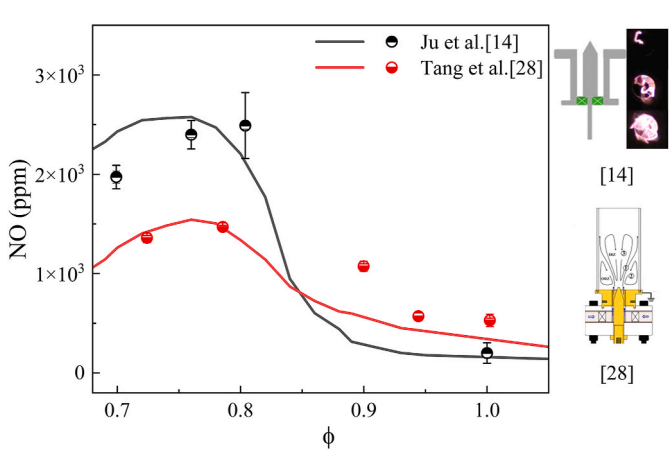

Fig. 4. Validation of NO emissions. (*line: numerical, symbol: experiment*).

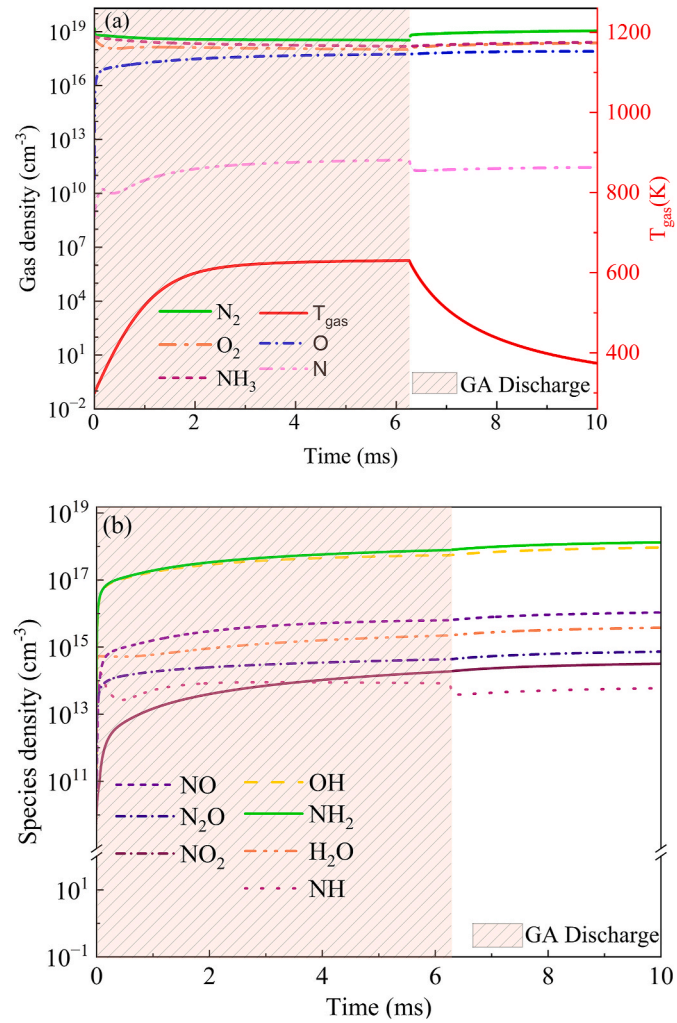

Fig. 5. Temporal evolution of species density and gas temperature for different main species. ($\phi = 1$, T = 300 K, P = 1 atm, E/N = 30 Td).

3.2. Behaviour of NH_3 in GAP

In this section, the behaviour of NH_3 ionization at different E/N is analysed and the pathways of NH_3 generation and consumption with GAP is discussed.

The temporal evolution of behavioural change of NH_3 during the plasma actuation are shown in Figs. 6 and 7. During the initial breakdown moment, NH_3 vibrates from the ground state to different excited states. Afterwards, the different excited states of NH_3 react with the initial gas components to form new NH_3 molecules. It is interesting to note that the excited states generated by the main vibrations of NH_3 at different energy injections (for different E/N) are all NH_3(v2). This is also consistent with the conclusions of Zheng et al. [37]. The rates of NH_3 (v4) and NH_3 (v13) production decrease slightly with increasing E/N. The generation rate is always smaller than the consumption efficiency, and the overall components show a decreasing trend. It means that in Fig. 7, the black line indicates that the reaction rate of NH_3 conversion to different vibrationally excited states of NH_3 is always more than the reaction rate of NH_3 generation indicated by the red line.

The pathway of NH_3 production and consumption is shown in Fig. 8 (a) and (b). It is observed that interconversion reactions between NH_3 and different excited states of NH_3 dominate the ionization phase as depicted in Fig. 8 (a). In addition to the interconversion of NH_3 with different excited states, there are further modes of consumption of NH_3 as shown in Fig. 8 (b). Reacting with different electronically excited

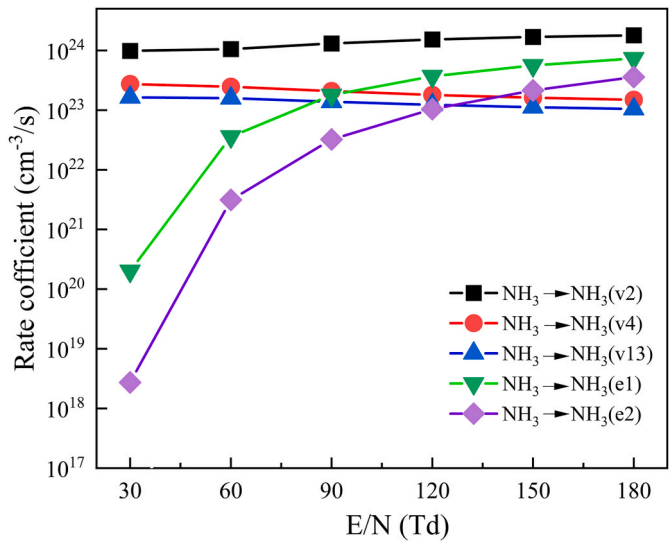

Fig. 6. Variation of electron reactions of NH_3 at different E/N (30 Td-180 Td).

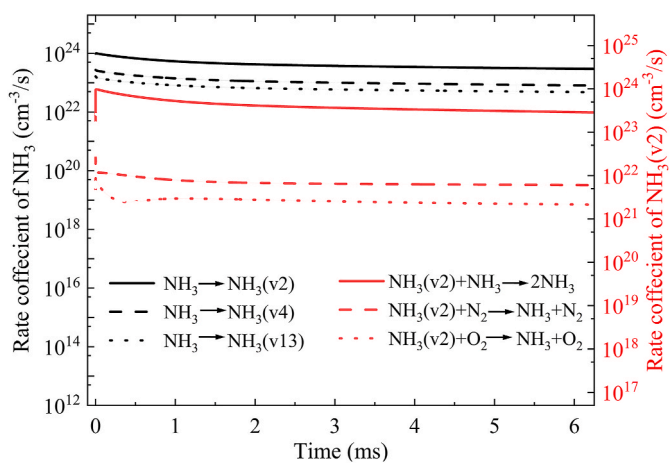

Fig. 7. Variation of rate coefficients of NH_3 and vibrationally excited state NH_3 during the GA discharge time at 30 Td.

states of N_2, nitrogen and oxygen atoms, dehydrogenate to form NH_2. This is one of the reasons for the higher production of NH_2 mentioned in 3.1. In parallel, the rate of reaction to produce is more significant in the discharge phase than in the no-discharge phase.

3.3. Generation of main groups affecting NO production

In this section, major radicals such as OH, NH, and NH_2 for NO generation and consumption with different E/N are discussed. This was taken as the reason for analysing the reduction in NO emissions when GAP promotes NH_3-air combustion.

The sensitivity analyses of the groups (OH, NH, NH_2) that play a primary role in NO production/consumption with plasma are shown in Fig. 9. According to Fig. 9 (a) and (c), NH_2 and NH, as the main pathways for NO consumption, show the strongest sensitivities to the reactions from NH_3 to NH_3(e1) and NH_3(e2), respectively. The electron collision reactions of NH_3 as affected by the strength of the electric field showed that the rate of the reaction to produce NH_3 in the different excited states increased rapidly with an increased E/N as illustrated in Fig. 6. This indicates that high field strength helps to promote the consumption path of NO. For the NH_2 generation reaction, the $O(^1D) + NH_3 \rightarrow OH + NH_2$ and $N_2(A) + NH_3 \rightarrow NH_2 + N_2$+H reaction dominates (30 Td). As E/N increases, $N(^2D) + NH_3 \rightarrow NH_2$+H + N_2 gradually takes the lead (52.1 % in 90 Td). Under low-temperature conditions, the thermal motion of molecules is reduced, and chemical reactions primarily rely on non-thermal processes (such as electron impact or the involvement of excited species). $N(^2D)$ and $O(^1D)$ loses energy through collisions with surrounding molecules or energy transfer, leading to the generation of intermediate radicals (e.g., OH and NH_2) [23]. Nevertheless, the increase of OH is often accompanied by the generation of NO, through HNO reactions. In Fig. 9 (b), the main pathway of OH formation is the reaction between H atoms and oxygen in different vibrational excited states.

3.4. Effect of GAP on combustion characteristics

In this section, sensitivity analyses and reaction pathways of NO in NH_3-air combustion under GAP were investigated. Previous experiments have shown that the maximum ϕ of NO change with plasma is between 0.8 and 0.9 [14,32], so this ϕ was selected for the present analysis.

The sensitivity analysis under plasma-assisted combustion versus pure combustion with path flux of NO is shown in Figs. 10 and 11. The sensitivity of plasma assisted combustion at different ϕ is approximately the same for the different reactions, the maximum sensitivity coefficients all occur in the reaction of HNO with H as shown in Fig. 10. The two reactions that consume NO show a significant magnitude of rate due to the generation of NH_2 and NH. The reaction $N + NO = N_2 + O$ at ϕ = 0.8 and 0.9 with sensitivity coefficients of 0.91 and 0.98. The rate increases due to the increase in N atoms produced by ionization, which contributes more to the consumption of NO.

Diversification of NO consumption paths at different ϕ (reactions $NH + H = N + H_2$, $HNO + OH = NO + H_2O$) attributed to plasma-generated intermediate groups. Similarly, in Fig. 11, combustion with or without

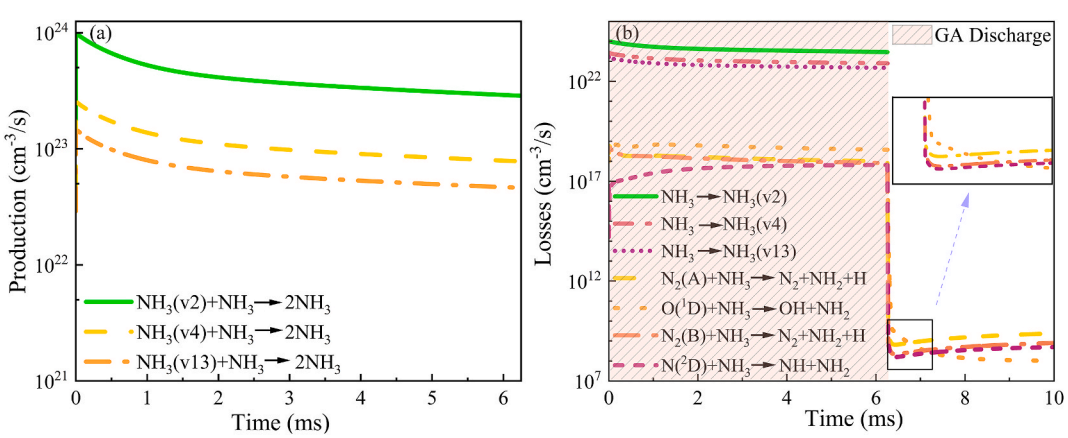

Fig. 8. (a) Production and (b) losses of NH_3 under GAP.

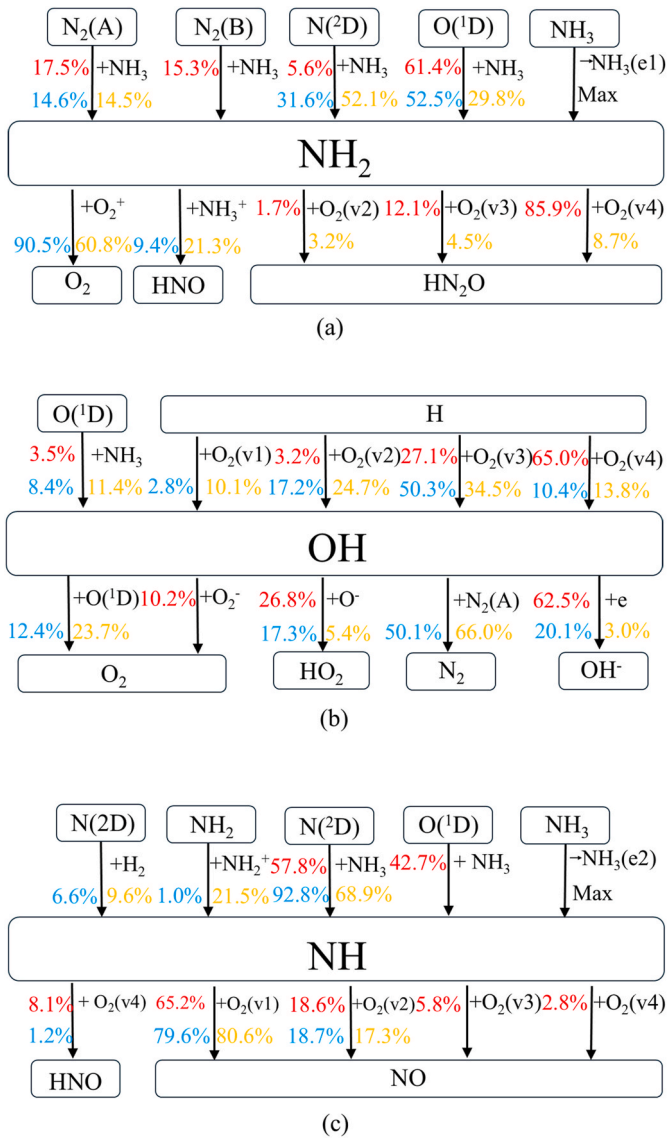

Fig. 9. Sensitivity analysis of (a) NH_2 (b) OH and (c) NH on the NO production at 30(red), 60(blue), 90(orange)Td in plasma. (*Numbers indicate the total reaction percentage*). (For interpretation of the references to colour in this figure legend, the reader is referred to the Web version of this article.)

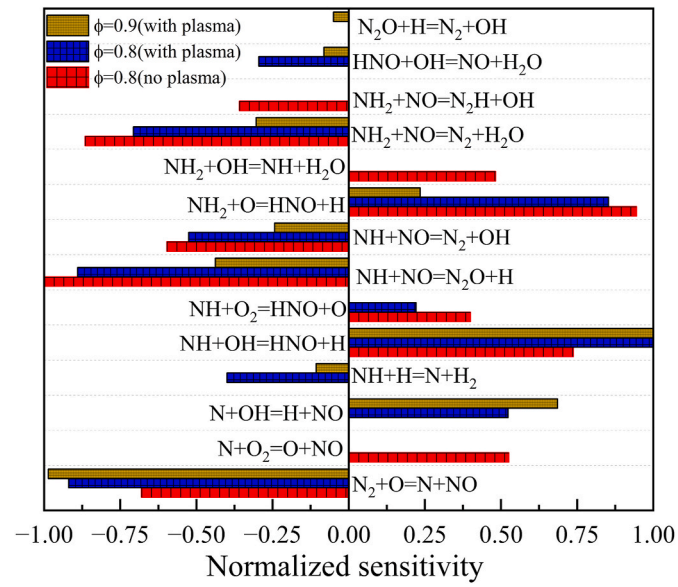

Fig. 10. Sensitivity analysis of NO production and consumption at $\phi = 0.8$ and 0.9.

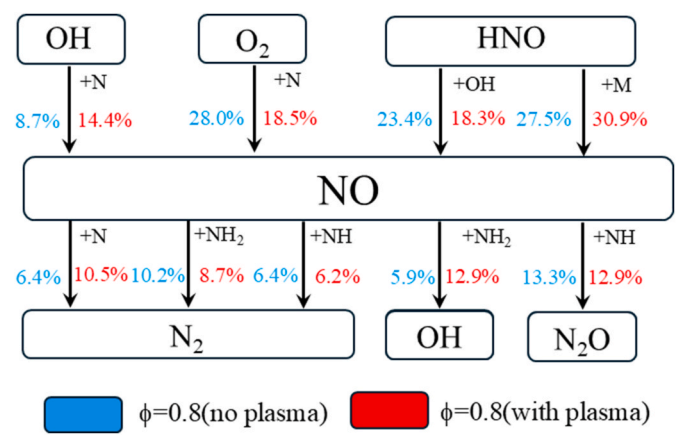

Fig. 11. Path flux of NO emissions at $\phi = 0.8$(with plasma and no plasma).

plasma, HNO is the main pathway for NO production, the same as that of literature [16,41]. Almost 50 % of NO is produced through the pathway of HNO with and without plasma. The percentage rate of production of NO consumed by NH_2 in GAP (12.9 %) is about twice as high as without GAP (5.9 %). Meanwhile, OH and N atoms are produced during the ionization phase, leading to the reaction OH + N=H + NO exacerbated by NO production with GAP (14.4 %, compared with 8.7 % without GAP).

4. Conclusion

This study presents a numerical model for predicting NO_x emissions during gliding arc plasma (GAP)-assisted combustion of an NH_3–air mixture. The NO production and consumption mechanisms under GAP actuation in NH_3-air mixtures are also investigated in detail. The main conclusions are summarized below:

(1) Three plasma reaction mechanisms for NH_3-air combustion were compared with the present GAP experiment. The mechanism of Mao et al. [23] was found to be optimal and was subsequently coupled with the Alnasif et al. [38] optimized combustion mechanism to develop a plasma-assisted combustion model.

(2) The results revealed that NO production primarily occurs via the HNO pathway, regardless of GAP actuation. The GAP Plasma reduces NO primarily by breaking down NH_3 into NH_2 (6.75 % in 30 Td), which enhances NO consumption, mainly through $N_2(A) + NH_3 \rightarrow NH_2 + N_2$+H and $O(^1D) + NH_3 \rightarrow OH + NH_2$.

(3) It is observed that higher plasma power further facilitates NO consumption. Strong electric fields promote the generation of excited ammonia states, which exhibit a higher tendency to form NH_2 and NH, enhancing NO reduction. NH_2 showed high sensitivity (52.1 %) to the reaction $N(^2D) + NH_3$ gNH_2+H + N_2, $N_2(A) + NH_3 \rightarrow NH_2 + N_2$+H. NH showed high sensitivity (68.9 %) to the reaction $N(^2D) + NH_3 \rightarrow NH_2$+NH (90 Td).

Future studies should take into account the influence of the swirling flame structure, the propagation of the arc within the GAP particularly the impact of arc rotation on spatial variations as well as other factors that may affect flame behaviour.

CRediT authorship contribution statement

Ziyu Wang: Writing – original draft, Methodology, Investigation, Formal analysis, Data curation, Conceptualization. **B. Aravind:** Writing – review & editing, Supervision, Methodology, Investigation, Conceptualization. **Syed Mashruk:** Writing – review & editing, Supervision. **Agustin Valera-Medina:** Writing – review & editing, Supervision, Funding acquisition.

Declaration of competing interest

The authors declare that they have no known competing financial interests or personal relationships that could have appeared to influence the work reported in this paper.

Acknowledgements

This work was supported by the European Union Project CAIPIRI-NH3A, under the GA Number 101191768. Views and opinions expressed are however those of the author(s) only and do not necessarily reflect those of the European Union or CINEA. Neither the European Union nor the granting authority can be held responsible for them. The research was undertaken at Cardiff University's Thermofluids Lab (W/0.17) with invaluable technical support from Mr. Jonathan Martin. For the purpose of open access, the author has applied a CC BY copyright licence to any Author Accepted Manuscript version arising. Information on the data underpinning this publication, including access details, can be found in the Cardiff University Research Data Repository at https://doi.org/10.17035/cardiff.30104149.v1.

Appendix A. Supplementary data

Supplementary data to this article can be found online at https://doi.org/10.1016/j.joei.2025.102314.

References

[1] C. Zamfirescu, I. Dincer, Using ammonia as a sustainable fuel, J. Power Sources 185 (1) (2008) 459–465.
[2] A. Valera-Medina, H. Xiao, M. Owen-Jones, W.I.F. David, P.J. Bowen, Ammonia for power, Prog. Energy Combust. Sci. 69 (2018) 63–102.
[3] B. Mei, X. Zhang, S. Ma, M. Cui, H. Guo, Z. Cao, Y. Li, Experimental and kinetic modeling investigation on the laminar flame propagation of ammonia under oxygen enrichment and elevated pressure conditions, Combust. Flame 210 (2019) 236–246.
[4] S. Mashruk, M.O. Vigueras-Zuniga, M.E. Tejeda-del-Cueto, H. Xiao, C. Yu, U. Maas, A. Valera-Medina, Combustion features of CH4/NH3/H2 ternary blends, Int. J. Hydrogen Energy 47 (70) (2022) 30315–30327.
[5] A. Valera-Medina, R. Marsh, J. Runyon, D. Pugh, P. Beasley, T. Hughes, P. Bowen, Ammonia–methane combustion in tangential swirl burners for gas turbine power generation, Appl. Energy 185 (2017) 1362–1371.
[6] R. Meloni, A. Valera-Medina, G. Babazzi, E. Pucci, S. Castellani, A. Andreini, Numerical investigation of the NOX emissions of a perfectly premixed NH3-H2 flame at moderate pressure levels, Fuel 385 (2025) 134128.
[7] H. Yamashita, A. Hayakawa, E.C. Okafor, S. Colson, K.D.K.A. Somarathne, T. Tsujimura, S. Ito, M. Uchida, T. Kudo, H. Kobayashi, Optimum primary equivalence ratio for rich-lean two-stage combustion of non-premixed ammonia/methane/air and ammonia/hydrogen/air flames in a swirling flow, Fuel 368 (2024) 131598.
[8] J. Davies, S. Mashruk, D. Sato, L. Mazzotta, D. Pugh, A. Valera-Medina, Emissions analyses of humidified cracked ammonia swirling flames, Combust. Flame 274 (2025) 113984.
[9] Y. Ju, W. Sun, Plasma assisted combustion: dynamics and chemistry, Prog. Energy Combust. Sci. 48 (2015) 21–83.
[10] Y. Ju, J.K. Lefkowitz, C.B. Reuter, S.H. Won, X. Yang, S. Yang, W. Sun, Z. Jiang, Q. Chen, Plasma assisted low temperature combustion, Plasma Chem. Plasma Process. 36 (1) (2016) 85–105.
[11] J. Tian, P. Liu, Z. Liu, J. Tang, W. Yin, Y. Cheng, Investigation on the effects of nanosecond pulsed discharge on combustion characteristics of C3H8/air mixtures using a rapid compression machine, J. Energy Inst. 119 (2025) 101983.
[12] T. Yu, H. Zhang, Z. Zhao, C. Kong, R. Zhang, J. Zhu, B. Zhou, Characteristics of an AC rotating gliding arc discharge in NH3 and air atmospheres, Phys. Plasmas 31 (2) (2024).
[13] H. Zhong, X. Mao, A.C. Rousso, C.L. Patrick, C. Yan, W. Xu, Q. Chen, G. Wysocki, Y. Ju, Kinetic study of plasma-assisted n-dodecane/O2/N2 pyrolysis and oxidation in a nanosecond-pulsed discharge, Proc. Combust. Inst. 38 (4) (2021) 6521–6531.
[14] R. Ju, J. Wang, M. Zhang, H. Mu, G. Zhang, J. Yu, Z. Huang, Stability and emission characteristics of ammonia/air premixed swirling flames with rotating gliding arc discharge plasma, Energy 277 (2023) 127649.
[15] J. Choe, W. Sun, T. Ombrello, C. Carter, Plasma assisted ammonia combustion: simultaneous NOx reduction and flame enhancement, Combust. Flame 228 (2021) 430–432.
[16] A.M. Elbaz, S. Wang, T.F. Guiberti, W.L. Roberts, Review on the recent advances on ammonia combustion from the fundamentals to the applications, Fuel Commun. 10 (2022) 100053.
[17] A.M. Radwan, M.C. Paul, Plasma assisted NH3 combustion and NOx reduction technologies: principles, challenges and prospective, Int. J. Hydrogen Energy 52 (2024) 819–833.
[18] R. Ju, J. Wang, M. Zhang, H. Mu, Y. Wu, G. Zhang, Z. Huang, Experimental study on burning velocity, structure, and NOx emission of premixed laminar and swirl NH3/H2/air flames assisted by non-thermal plasma, Appl. Energy Combust. Sci. 14 (2023) 100149.
[19] G. Faingold, J.K. Lefkowitz, A numerical investigation of NH3/O2/He ignition limits in a non-thermal plasma, Proc. Combust. Inst. 38 (4) (2021) 6661–6669.
[20] M. Shahsavari, A.A. Konnov, A. Valera-Medina, M. Jangi, On nanosecond plasma-assisted ammonia combustion: effects of pulse and mixture properties, Combust. Flame 245 (2022) 112368.
[21] X. Mao, A. Rousso, Q. Chen, Y. Ju, Numerical modeling of ignition enhancement of CH4/O2/He mixtures using a hybrid repetitive nanosecond and DC discharge, Proc. Combust. Inst. 37 (4) (2019) 5545–5552.
[22] H. Zhong, X. Mao, N. Liu, Z. Wang, T. Ombrello, Y. Ju, Understanding non-equilibrium N2O/NOx chemistry in plasma-assisted low-temperature NH3 oxidation, Combust. Flame 256 (2023) 112948.
[23] X. Mao, H. Zhong, N. Liu, Z. Wang, Y. Ju, Ignition enhancement and NOx formation of NH3/air mixtures by non-equilibrium plasma discharge, Combust. Flame 259 (2024) 113140.
[24] T.S. Taneja, P.N. Johnson, S. Yang, Nanosecond pulsed plasma assisted combustion of ammonia-air mixtures: effects on ignition delays and NOx emission, Combust. Flame 245 (2022) 112327.
[25] M. Shahsavari, A.A. Konnov, X.-S. Bai, A. Valera-Medina, T. Li, M. Jangi, Synergistic effects of nanosecond plasma discharge and hydrogen on ammonia combustion, Fuel 348 (2023) 128475.
[26] Y. Qiu, Y. Zhu, Y. Wu, N. Zhao, Z. Li, M. Hao, B. Zhang, D. Pan, Numerical investigation of the hybrid pulse–DC plasma assisted ignition and NOx emission of NH3/N2/O2 mixture, Combust. Flame 258 (2023) 113078.
[27] Z. Xin, X. Li, Z. Zheng, Y. Hu, R. Cao, A. Sun, F. Zhao, W. Yu, Study on the kinetics and energy transfer during ignition of methane excited by NRP-SDBD non-equilibrium plasma, J. Energy Inst. 118 (2025) 101929.
[28] Y. Tang, D. Xie, B. Shi, N. Wang, S. Li, Flammability enhancement of swirling ammonia/air combustion using AC powered gliding arc discharges, Fuel 313 (2022) 122674.
[29] Z. Wang, B. Aravind, S. Mashruk, A. Valera-Medina, Experimental investigation on the effects of gliding arc plasma on the combustion characteristics of air stratified NH3 flames, Energy (2025) 138413.
[30] J. Cui, Z. Xu, J. Zhang, Q. Nie, G. Xu, L. Ren, Online diagnosis of electron excitation temperature in CH4+H2 discharge plasma at atmospheric pressure by optical emission spectra. Science in China series G: physics, Mech. Astron. 51 (12) (2008) 1892–1896.
[31] L.W.S. Crispim, P.H. Hallak, M.S. Benilov, M.Y. Ballester, Modelling spark-plug discharge in dry air, Combust. Flame 198 (2018) 81–88.
[32] B. Aravind, Z. Wang, Syed Mashruk, Deanna A. Lacoste, A. Valera-Medina, Novel Strategy for Combustion Enhancement of NH3-air Mixture Using Gliding Arc Plasma, vol. 41, Proceedings of the combustion institute, 2025.
[33] D.P. Subedi, R.P. Guragain, U.M. Joshi, Surface modification of polymers by 50 Hz dielectric barrier discharge (DBD) plasma produced in air at 40 Torr, Fund. Plasma Phys. 10 (2024) 100058.
[34] G. Dong, Y. Zhou, P. Ming, Z. Wu, H. Chen, Y. Huang, L. Li, Kinetics-Based analysis of the gliding arc plasma assisted ammonia decomposition process towards vehicle on-board applications, Chem. Eng. J. 505 (2025) 159443.
[35] S. Pancheshnyi, B. Eismann, G. Hagelaar, L. Pitchford, Computer Code Zdplaskin, University of Toulouse, LAPLACE. Tech. Rep, CNRS-UPS-INP, Toulouse, France, 2008.
[36] R.J. Kee, F.M. Rupley, E. Meeks, J.A. Miller, CHEMKIN-III: a FORTRAN Chemical Kinetics Package for the Analysis of Gas-phase Chemical and Plasma Kinetics, 1996.
[37] Z. Zheng, C. Wang, Z. Xin, Y. Hu, Q. Zhu, W. Yang, F. Zhao, W. Yu, Kinetic modelling of non-equilibrium plasma enhanced catalytic ammonia decomposition, J. Energy Inst. 116 (2024) 101715.
[38] A. Alnasif, S. Mashruk, M. Hayashi, J. Jójka, H. Shi, A. Hayakawa, A. Valera-Medina, Performance investigation of currently available reaction mechanisms in the estimation of NO measurements: a comparative study, Energies 16 (9) (2023) 3847.

[39] A. Alnasif, J. Jójka, M. Papp, A.G. Szanthoffer, M. Kovaleva, T. Turanyi, A. Valera Medina, T. Nagy, Compact Kinetic Model for the Combustion of NH3/H2 Mixtures, J Ammonia Energy, 2025.
[40] R. Parajuli, S. Matt, A. Stamatovic, T.D. Märk, P. Scheier, Unimolecular dissociation of non-stoichiometric oxygen cluster ions On+* (n=5, 7, 9, 11): a switch from O3 to O2 loss above cluster size n=5, Int. J. Mass Spectrom. 220 (2) (2002) 221–230.
[41] S. Mashruk, H. Shi, L. Mazzotta, C.E. Ustun, B. Aravind, R. Meloni, A. Alnasif, E. Boulet, R. Jankowski, C. Yu, M. Alnajideen, A. Paykani, U. Maas, R. Slefarski, D. Borello, A. Valera-Medina, Perspectives on NOX emissions and impacts from ammonia combustion processes, Energy Fuel. 38 (20) (2024) 19253–19292.